Self-air-cooling Design and Optimization for an Outer-rotor PMSG in External Still Air

Sirui Wang, *Student Member, IEEE*, Fangrui Wei, Yong Li, Jianhui Hu,
Qian Wang, *Member, IEEE*, and Pengcheng Ma

***Abstract*—For hybrid-electric unmanned aerial vehicles (UAVs), the stable power supply from the onboard permanent magnet synchronous generator (PMSG) is critical. Overheating in the confined compartment can directly lead to power interruption and system failure. Therefore, proactively improving the thermal management is not only a key technical prerequisite for ensuring flight reliability and mission success, but also enhances the machine's efficiency and the overall power density of the system. Targeting the stringent spatial constraints in UAV applications, novel self-air-cooling heat dissipation topologies are investigated and highlighted on the rotor sidewall for compact outer-rotor generators. A systematic optimization framework, centered on a multi-objective genetic algorithm, is developed to Pareto-optimize the fin geometries, balancing thermal performance against aerodynamic penalty. The proposed topologies are innovatively deployed on the rotor sidewall, uniquely combining the structural space of an outer-rotor machine with self-air-cooling to generate directed airflow of varying patterns that directly enhance the cooling efficiency of the stator. The parameters of the designed self-air-cooled heat dissipation topologies are optimized via a multi-objective genetic algorithm. A temperature rise test under windless conditions shows that the proposed self-air-cooled structure reduces the stator temperature of the generator by 37.1 ℃ at 5000 r/min, confirming the effectiveness and engineering feasibility for practical applications..**

***Index Terms*—External still air, Hybrid power system, Heat dissipation structures, Outer-rotor permanent magnet synchronous generator (PMSG), Rotor sidewall, Self-air-cooling, Unmanned aerial vehicles (UAVs).**

I. INTRODUCTION

THE growing use of unmanned aerial vehicles (UAVs) has elevated the permanent magnet synchronous generator (PMSG), the key power unit, to a prominent research topic. Enhancing the power density and reliability of PMSGs is therefore a central design objective. The spatial constraints of drone platforms, however, limit cooling options, which intensifies the challenges associated with generator thermal management [1].

Enhancing generator cooling necessitates the adoption of cooling methods compatible with the operational environment. Oil spray cooling represents a direct thermal management approach. In [2] and [3], oil is atomized through nozzles and sprayed onto the end windings, enabling direct cooling of this highest-temperature region. However, the spray cooling system entails auxiliary components such as pumps, nozzles, and tanks, making it more suitable for medium and large-sized machines with high power density. In [4], an alternative method is presented, where oil is directly injected into channels within the rotor.

Apart from oil cooling, other fluid-based and passive cooling techniques have been explored. The heat pipe is a passive, two-phase heat transfer device that operates on the phase change cycle of a sealed working fluid. One approach, as seen in [5]-[7], is to install heat pipes in areas of the stator yoke with sparser magnetic flux lines, thus minimizing impact on electromagnetic performance. Another strategy, detailed in [8]-[11], involves inserting heat pipes directly into the stator windings, which positions them closer to the heat source for effective cooling, albeit at the cost of compressing the winding areas and reducing the machine's electrical load.

Despite the high cooling efficiency offered by heat pipes, air cooling remains a favored choice in many small and medium-sized motor applications. This preference stems primarily from the system's simplicity and the consequent reduction in maintenance requirements. In [12]-[14], forced air cooling is achieved using external fans. Internally designed ventilation channels facilitate air circulation, effectively dissipating machine-generated heat. In such configurations, airflow typically follows an axial path into or out of the machine.

In constrained applications such as hybrid-electric UAVs, the use of external forced air-cooling for outer-rotor PMSG (OR-PMSG) is often precluded by design or operation. Consequently, reliance shifts to internal cooling methods for thermal management of components like integrated starter-generators (ISGs). In [15]-[16], the stator yoke is filled with thermally conductive materials to enhance heat dissipation at the stator end. In [17], thermally conductive elements connected to the stator yoke are inserted into the stator slots to accelerate heat transfer from the windings.

Manuscript received December 27, 2025; revised January 29, 2026; accepted February 12, 2026. Date of publication March 25, 2026; Date of current version March 20, 2026.

This work was supported in part by the State Key Laboratory of Robotics and System under Grant SKLRS202407B.

Sirui Wang, Fangrui Wei, Yong Li, Jianhui Hu, and Qian Wang are with the Department of Electrical Engineering, Harbin Institute of Technology, Harbin, Heilongjiang 150001, China. (e-mail: wsr53@stu.hit.edu.cn; weifangrui@hit.edu.cn; liyong611@hit.edu.cn; hujianhui@hit.edu.cn; q.wang@hit.edu.cn)

Pengcheng Ma is with the Information Research Institute, Chinese Academy of Sciences, Beijing 100864, China. (e-mail: mpc61hit@126.com)

(*Corresponding Author*: *Fangrui Wei*)

Digital Object Identifier 10.30941/CESTEMS.2026.00006

Since passive cooling exhibits limited effectiveness in external still air, thermal design has increasingly focused on active solutions. A prominent method involves utilizing rotor rotation, leveraging the principle of axial flow fans in structural design to enhance stator cooling. In [18], a self-pumping air-cooling design based on the principle of a centrifugal fan is applied to a 1 MW high-speed motor. In the structure, the fan is located on the side wall of the rotor, with openings on the outer wall of the rotor. In [19], a detailed analysis of the parameters of the stator cooling channels for the self-pumping structure is conducted. In [20], two centrifugal fans are installed on both sides of a 3 kW, 300 r/min motor. The self-pumping structure requires considerable space, which may limit its applicability in constrained environments.

Another rotor-rotation-enhanced cooling method is the blade-type fan design. In [21], an axial fan with a propeller-like shape is combined with a rotor to enhance the cooling of low-speed, high-torque motors, thereby significantly increasing the torque density of the motor. In [22], large fan blades are mounted on both sides of the machine to generate airflow around the windings, which significantly improves winding cooling, with considerable space occupation. In [23], an axial fan driven by rotor rotation is utilized for machine cooling. The concept is similar to the approach proposed in this paper; however, the present study focuses on high-power-density machines for UAV applications, where the cooling structure is integrated into the sidewall of the machine rotor.

Although research on rotor-rotation-enhanced cooling is well-established for large-scale electric machines, it remains limited for applications in confined spaces such as hybrid-electric UAVs. Most air-cooled machines depend on additional forced-air cooling facilities, which occupy considerable space. Although some designs incorporate optimized cooling features, they often exhibit relatively low utilization of the rotor's inherent potential. Furthermore, existing self-cooling designs typically involve mounting large fans at both ends of the machine. This approach results in a bulky configuration and excessive spatial footprint, rendering it unsuitable for applications in UAVs where space is at a premium.

The main contributions and innovations in this paper are summarized as follows.

1) Proposal of several novel and effective self-air-cooling structures integrated directly onto the rotor sidewall.

2) Demonstration that the proposed structures offer significantly superior cooling performance compared to open-hole dissipation methods, while occupying minimal space.

3) Experimental validation confirming that the core principle of the proposed self-cooling approach is effective and offers a promising solution for thermal management in small-scale, high-power-density outer-rotor generators.

The remainder of this work is structured as follows: Section II presents the key parameters and models of the generator under study. A fluid–thermal–structural coupling method is employed to establish baseline parameters for optimization. Section III introduces two distinct self-cooling structures integrated into the rotor sidewall and details the optimization of the critical parameters. Section IV verifies the thermal dissipation performance of the proposed mechanism through an experimental platform. Finally, Section V provides concluding remarks.

II. Generator Parameters and Model

A. Parameters and Model of Researched OR-PMSG

The key parameters of the OR-PMSG utilized in this paper are listed in Table I. The machine is an ISG designed for small engines, with an operational speed of 5000 r/min.

The topology of the OR-PMSM is illustrated in Fig. 1. Although the outer-rotor design offers high torque density, it also leads to concentrated heat buildup in the stator, complicating heat dissipation. Consequently, the stator windings are encapsulated into a single unit with grooved outer surfaces to increase the cooling area. To address this, self-air-cooling structures are implemented at the winding ends, leveraging the rotor's rotation to generate the required airflow.

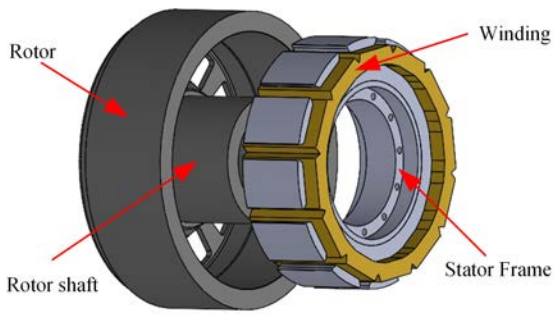

Fig. 1. Structure of the researched OR-PMSG.

TABLE I
SPECIFICATIONS OF OR-PMSG

Parameters	Value
Rated power/kW	3.5
Rated speed/(r·min^{-1})	5000
Outer diameter/mm	144
Inner diameter/mm	66
Number of slots	20
Number of poles	18
Air gap length/mm	1.6

The simulation model is identical to the model shown in Fig. 1, with the winding (including enameled wire, slot insulation, and potting compound) equivalently modeled as an integrated solid heat source.

The computational fluid dynamics (CFDs) analysis employs the standard turbulent kinetic energy (k)-turbulent dissipation rate (ε) model with the energy equation activated to resolve the temperature field. A pressure-based solver is utilized, defining the inlet and outlet boundaries with zero-gauge total pressure. The ambient temperature is maintained at 16 °C. For heat generation, the copper loss is modeled as a uniform volumetric source within the windings, and the iron loss is uniformly distributed over the stator core and rotor volumes. The aerodynamic windage loss generated by the rotating fins is not explicitly added as a volumetric heat source. To ensure a valid comparison, all conditions except

for the rotor's cooling structure are kept identical across the analyses.

B. Influences of Traditional Ventilation Holes

As a comparative benchmark, the steady-state results of the fluid-solid-thermal coupled field are first calculated for the baseline model without any additional cooling structures. To quantify the cooling effectiveness, three key metrics are defined: The average wind speed on a plane a specific distance from the stator's non-lead-out end (adjacent to the rotor)—a location chosen for the proximity to the stator and because it lies clear of the designed fins—is designated as the stator wind speed; the average temperatures of the stator's left and right end faces are defined as T_{SA} and T_{SB}, respectively. The three parameters served as the evaluation criteria.

Enhancing cooling by incorporating ventilation holes in the generator casing is a common practice in air-cooled generators to reduce stator temperature. However, this method is unsuitable without external forced cooling. The calculation results for this ventilation hole configuration without external forced cooling, accounting for the impact on the rotor wall, are presented in Table II.

TABLE II
REFERENCE TEMPERATURE OF OR-PMSG

Rotor status	Wind speed/(m·s^{-1})	T_{SA}/°C	T_{SB}/°C
No ventilation holes	1.54	163.1	164.0
With ventilation holes	1.62	160.3	161.1

The analysis reveals that without external forced cooling, the contribution of sidewall ventilation holes to the internal wind speed is minimal. The rotational motion of the rotor fails to induce a coherent axial flow through these holes. The wind speed distribution diagram for this structure at 5000 r/min in Fig. 2 clearly demonstrates the lack of directed airflow. The concomitant consistency in both simulated wind speed and temperature results confirms the flow ineffectiveness. Under the same thermal load, a smooth rotor yields a steady-state temperature similar to the ventilation hole design. Therefore, it can be concluded that for rotor sidewall ventilation holes of similar surface area, the ultimate impact on temperature reduction is functionally equivalent to the baseline configuration without any holes.

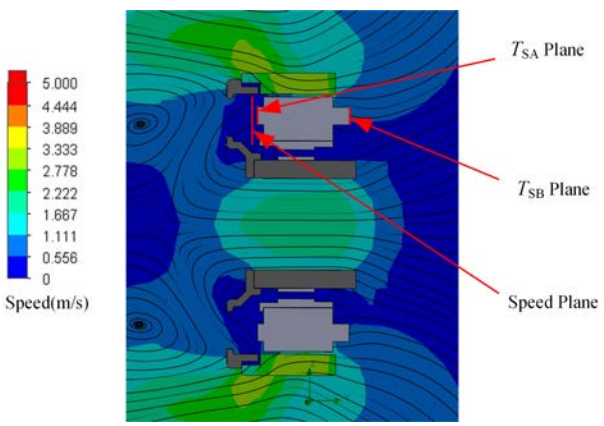

Fig. 2. Wind speed distribution diagram of ventilation holes.

III. PROPOSED SELF-AIR-COOLING STRUCTURES

A. Improved Built-in Fins on Rotor Side Wall

Although prior approaches, such as the housing-mounted fin in [21], enhance rotor heat dissipation, the rotational kinetic energy of the rotor remains underutilized. A novel design of built-in fins installed directly on the rotor sidewall is proposed in this paper. As illustrated in Fig. 3, these fins are mounted on the inner surface, with the inner and outer radii of R_o and R_i, respectively. The operation harnesses the rotor's rotation to accelerate airflow in the gap between the rotor and the stator end face. The optimization targets three key performance metrics: system mass m_{bi}, aerodynamic power loss P, and the operating temperature T_{bi} of the stator. The selection is directly motivated by the stringent requirements of UAV applications. The design aims to achieve paramount stator cooling within stringent spatial and operational (rated speed) limits, concurrently achieving an optimal trade-off between absorbed fin power and additional mass.

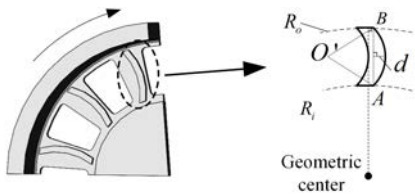

Fig. 3. Structure of the built-in fins.

The cooling performance of these fins is directly governed by their structural parameters. The most influential design variables are the number of fins (n), the fin height (h), and the offset distance (d). For intuitive analysis, the arc's offset distance d—defined as the spacing between the outermost and the innermost edges of the curved fin—is used as an independent variable instead of the arc radius. The fin geometry is defined as follows: If d = 0 mm, it is a standard cuboid; otherwise, it features an arc whose radius R_C is calculated as (1):

$$R_c = \frac{(R_o - R_i)^2}{8d} + \frac{d}{2} \tag{1}$$

The analysis is based on the following assumptions: The gas is incompressible with constant density, the flow is quasi-steady, and transient effects are neglected. Based on the assumptions, the fin is divided into infinitesimal elements along the radial direction. The drag force F_d on an element located at radius r is:

$$F_d = \frac{1}{2}\rho_{air} h C_d(\omega, d)^2 \, dr \tag{2}$$

where ρ_{air} is the air density, the drag coefficient C_d is considered a function of the blade offset distance (d) and the Reynolds number (ω). The torque exerted by the drag M_d on the rotor is:

$$M_d = r \cdot F_d = \frac{1}{2} C_d^2 (R_o - R_i) hr \cdot dr \tag{3}$$

The aerodynamic power loss P is given by:

$$P = nM_d\omega = \frac{n}{8}\rho_{air} C_d \omega^3 h (R_o - R_i)(R_o^3 - R_i^3) \tag{4}$$

To determine the added mass of the fins, the arc length s_{bi} must first be found:

$$s_{bi} = R_c\theta_s = 2R_c \arcsin\left(\frac{R_o - R_i}{2R_c}\right) \tag{5}$$

where θ_s is the central angle of the arc AB, therefore, total mass m_{bi} is given by:

$$m_{bi} = 2n\rho_{bi}hl_{bi}R_c \arcsin\left(\frac{R_o - R_i}{2R_c}\right) \tag{6}$$

where ρ_{bi} is the density of built-in fins, and l_{bi} is the length of the fins.

The baseline configuration for the parametric study is defined with an initial fin count of 12, an offset distance d of 3.7 mm, and a fin height h of 4 mm. Each parameter is varied individually while keeping the others at their baseline values. The resulting performance under different parameter sets is shown in Fig. 4.

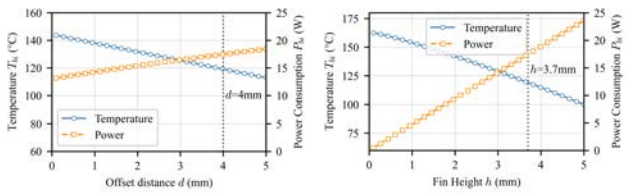

(a) (b)

Fig. 4. Resulting performance under these different parameter sets. (a) Performance under different distance *d*. (b) Performance under different distance *h*.

Fig. 4 illustrates the effects of varying fin height h and offset distance d on the the operating temperature T_{bi} and the power consumption P_{bi}. The trends clearly show that increasing h significantly enhances heat dissipation T_{bi} but at the cost of a rapidly increasing P_{bi}. Similarly, increasing d improves cooling up to a point, beyond which the flow passage becomes too restricted, leading to diminished returns in cooling and a sharp rise in P_{bi}.

Due to the complex, non-explicit relationship between stator temperature and the fin's three design parameters, a surrogate model based on a covariance-function-form radial basis formulation (RBF) is constructed and fitted to CFD simulation data. The chosen covariance kernel is expressed as:

$$k(x,x') = \sigma_f^2 \exp\left(-\frac{1}{2}\sum_{i=1}^{3}\frac{(x_i - x_i')^2}{l_{ki}^2}\right) + \sigma_n^2\delta(x,x') \tag{7}$$

where c =1.3225 represents the signal variance, σ_n^2 = 0.018 denotes the noise variance, and l_k = [2.11, 0.709, 1.79] are the characteristic length scales for design parameters [*d*, *n*, *h*], respectively. The fitting effect is shown in Fig. 5.

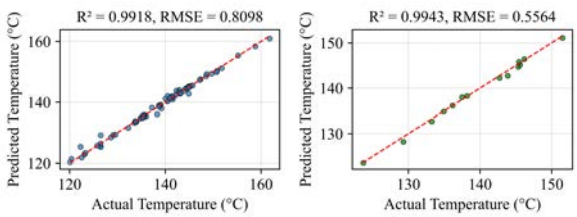

(a) (b)

Fig. 5. The fitting effect of RBF. (a) Training set. (b) Testing set.

As demonstrated in Fig. 5, the constructed RBF model fully leverages the CFD simulation results, effectively capturing the variation trend of stator temperature T_{bi} with respect to the three design parameters. This approach enables an accurate estimation of the fin's heat dissipation performance.

The multi-objective optimization is performed utilizing the non-dominated sorting genetic algorithm-II (NSGA-II), which employs a natural selection mechanism to simultaneously optimize competing objectives. The algorithm parameters include a population of 100 evolving over 200 generations, with crossover and mutation probabilities set to 0.8 and 0.2, respectively. As a convergence acceleration strategy, 30% of the initial population is seeded with solutions from prior experimental data, with the rest initialized randomly.

The Pareto front resulting from the optimization is presented in Fig. 6, with a selected optimal point marked for further analysis.

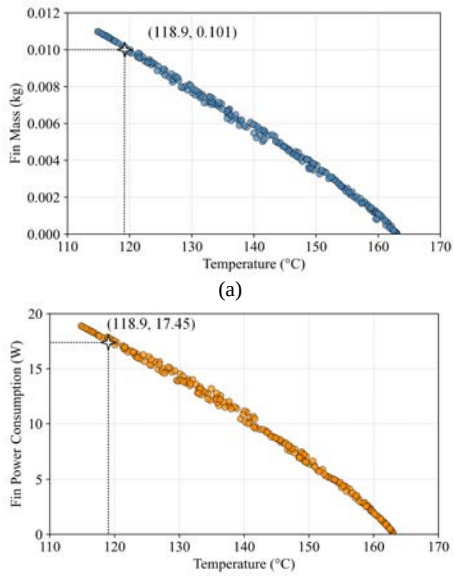

(a)

(b)

Fig. 6. Pareto front resulting. (a) Mass–temperature relationship. (b) Power consumption–temperature relationship.

The final selection of a design point for a specific application involves practical considerations such as manufacturability, structural integrity, and integration constraints. The selected design from the Pareto front is subjected to a rigorous CFD simulation for validation. As shown in Fig. 6, the simulation results show close agreement with the predictions from the RBF surrogate model, confirming the accuracy of the optimization framework and the feasibility of the final design.

B. Novel Composite Fins on Rotor Side Wall

Prior research has explored using large fan blades or rotor-mounted structures for cooling [19], but these often require substantial dimensions that compromise structural and electromagnetic performance. In contrast, the composite fins proposed in this study are compactly integrated into the rotor sidewall ventilation holes. Positioned directly opposite the stator windings with minimal spatial occupancy, they avoid the drawbacks of conventional designs.

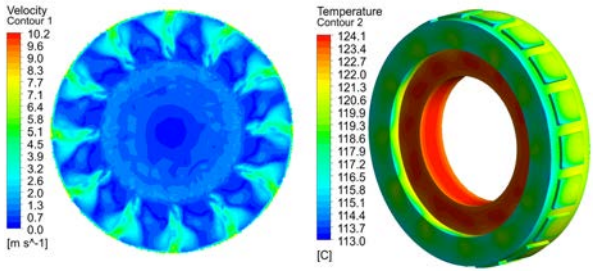

(a) (b)

Fig. 7. Cooling performance of the optimized built-in fins. (a) Wind speed. (b) Temperature of stator.

Unlike previously described built-in fins, the composite fins utilize the rotor sidewall thickness to maximize blade length, effectively acting as axial flow impellers. During operation, they generate directed axial airflow to actively cool the entire stator.

At the system level, cooling air enters through ventilation holes on one rotor side. Driven by pressure from the rotating fins, it is forced through intentionally designed gaps in the stator potting compound, passes through the air gap, and finally exits the stator from the opposite end.

For the stator, the assembly of the composite fins and the rotor effectively constitutes a medium-speed, low-pressure fan operating at 5,000 r/min. The detailed blade structure of this integrated system is illustrated in Fig. 8.

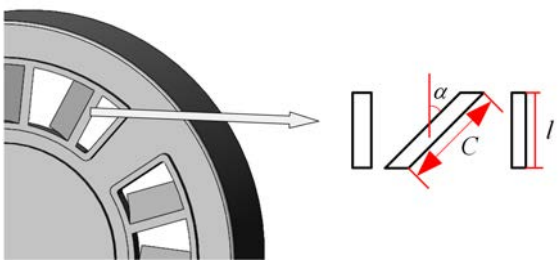

Fig. 8. Structure of the composite fins.

The number of fins is a critical design parameter. Under the constraint of a constant total ventilation hole area on the rotor sidewall, increasing the number of fins directly reduces the open area available for cooling air intake. This reduction in the inflow area becomes the primary bottleneck, limiting the system's overall heat dissipation capacity.

The assumptions underlying the fluid-structure interaction analysis of composite fins are the same as those for built-in fins. Inspired by [24], the blade angle, denoted as α, is defined as the deflection angle of the fin at a given cross-section. This angle directly determines the pressure head generated by the airflow at a constant rotational speed. However, due to the geometric limitation imposed by the short fin length, the feasible range for adjusting this deflection angle is constrained. For a single fin, the chord length C can be expressed as (8):

$$C = \frac{l}{\cos\alpha} \tag{8}$$

Due to the rotational nature of the system, the tangential velocity of the airflow over the fins increases linearly with the radius. Consequently, the relative inflow velocity and effective angle of attack vary along the blade span from the root to the tip. To ensure efficient operation across the entire fin, the blade angle must be carefully designed as a function of the radius. Based on fundamental principles of fluid mechanics, the lift force per unit span, $L(r)$, at a given radial position can be expressed as (9):

$$L(r) = \rho_{air}\omega^2 r^2 C \sin 2\alpha dr \tag{9}$$

where ω is the rotational speed of the generator.

Unlike conventional axial-flow fins, the composite fins simultaneously generate axial and circumferential airflow within the stator-rotor cavity. This combined flow, visualized in Fig. 9 for α = 45°, enhances cooling by improving heat transfer beyond the contribution of axial flow alone.

Governed by mass conservation, the mass flow rate driven by the fins is constant throughout the system. Following the earlier assumption, air is considered an incompressible gas. The overall volumetric flow rate Q can be determined using the continuity equation. Defining A_1 and v_1 as the total area and axial velocity at the rotor vents, and A_2, v_2 for the stator and air gap, the flow rate is given by (10):

$$Q = v_1 A_1 = v_2 A_2 \tag{10}$$

Since the cross-sectional area A_1 is a constant across all designs, the axial velocity v_1 at the stator interface becomes the decisive parameter for comparing axial flow drive capacity. This is because v_1 alone dictates the volumetric flow rate in this fixed area, representing the core output of the fin's pumping action. Therefore, v_1 can be directly used to evaluate their contribution to the overall cooling performance.

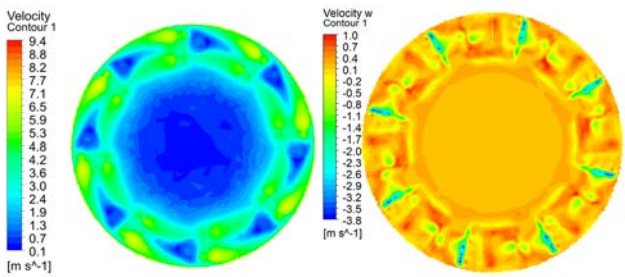

(a) (b)

Fig. 9. Wind speed distribution when α is 45°. (a) Airflow velocity distribution. (b) Axial velocity distribution.

At a swing angle α of 0°, the composite fin is equivalent to a built-in fin with a length of 2.5 mm. Theoretically, the effective range for α is from 0° to 45°, as derived from (9), which predicts a reduction in lift beyond 45°.

To practically investigate the influence of swirling flow and structural constraints, the study scope is expanded to 50°. Fig. 10 presents the resulting average axial velocity (v_a) and average overall velocity (v_s) at the stator end section for different α values within this range.

The results demonstrate a greater influence of v_s on stator temperature compared to v_a. This is further illustrated by the temperature increase observed when α rose from 45° to 50°—a condition in which v_a actually increased. Nevertheless, the superior cooling performance of the composite fins is confirmed, as they achieve a lower stator temperature than the built-in fins under the same thermal load.

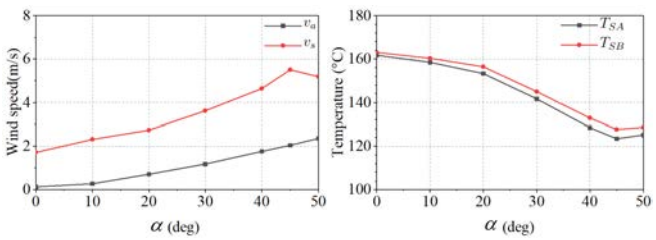

(a) (b)

Fig. 10. Cooling performance at different α. (a) Wind speed distribution. (b) Temperature of stator.

Moving beyond the simple flat blades used in prior studies, our subsequent research will apply traditional aerodynamic design methods to optimize the blade geometry. The design freedom, however, is constrained by the finite area and chord length permissible within the rotor's ventilation holes.

In fin design, it is essential to maintain a uniform axial flow velocity across all radial positions to ensure structural integrity. Using the v_1 through the composite fins as a reference, the flow velocity coefficient at any given radius is defined as a function of λ:

$$\lambda = \frac{v_1}{\omega r} \tag{11}$$

Then calculate the swirl coefficient ε_s at each radius:

$$\varepsilon_s = K\frac{\lambda}{2} \tag{12}$$

where K is a constant determined by design experience and optimal scheme selection. In this way, the angle β_m between the resultant velocity of the airflow and the rotational axis can be expressed as (13):

$$\tan\beta_m = \frac{1-\frac{1}{2}\varepsilon_s\lambda}{\lambda} \tag{13}$$

The lift coefficient C_L of the fin at different radii can be obtained as (14):

$$C_L = \frac{\pi r}{3C}\varepsilon_s\cos\beta_m - \frac{\pi r}{30C}K\cos^2\beta_m\sin\beta_m \tag{14}$$

The NACA 6409 airfoil is chosen from a standard database for the high lift. Analysis of the lift coefficient curve led to the selection of a ε_s = 12°. Accordingly, the blade angle α can be calculated by a function of the radius:

$$\varepsilon = 90° + \alpha - \beta_m \tag{15}$$

The fin structure resulting from the aforementioned design process is presented in Fig. 11. Table III compares the thermal performance of the newly designed airfoil fins against the flat-bladed fins under identical conditions. The flat-plate fin configuration selected for this comparison is the highest-performing variant, which features a α of 45°.

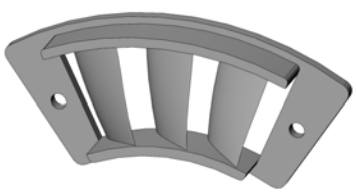

Fig. 11. Composite fin structure after aerodynamic design.

TABLE III
CALCULATION RESULTS OF DIFFERENT SHAPE FOR COMPOSITE FINS

Fin structure	v_a /(m·s^{-1})	v_s /(m·s^{-1})	T_{SA}/℃	T_{SB}/℃
Flat-plate	2.04	5.50	119.4	122.7
Airfoil design	2.31	5.74	115.3	118.6

The empirical evidence establishes that the aerodynamic design of the fin is paramount for the self-cooling performance of the composite structure. The airfoil profile boosts the cooling wind speed on the stator end surface by 4 °C despite maintaining an identical fin size. This results in a remarkable average temperature reduction of 43.8 °C relative to an uncooled configuration. Compared to the effective flat-plate fin, it achieves a further 9.1% reduction in temperature rise, highlighting the superiority of the optimized shape.

IV. EXPERIMENTAL VERIFICATION

A. Experimental Platform

The cooling effectiveness is verified using a 3.5 kW outer-rotor PMSM equipped with the designed fins (Fig. 12). The composite fins are fabricated using the carbon fiber-reinforced nylon, produced using three-dimensional (3D) printing, and the total mass of the complete set of 5 attached fins is measured to be 20 g. Composite fins are screwed into the rotor's ventilation openings, and built-in fins are fixed to the side walls.

Stator temperature is measured with an infrared thermal imager (range: –25 to +550 °C, accuracy: ±1 °C), which tracked and recorded temperatures at the field-of-view center, maximum, and minimum points.

(a) (b)

Fig. 12. Experimental equipment. (a) Generator with built-in fins. (b) Generator with composite fins.

The experimental platform (Fig. 13) utilizes a prime motor to drive the generator. Input power is calculated from torque and speed measurements taken between them. The generator's output is loaded via a rectifying controller onto a power resistor. To simulate actual generator operating conditions, the test setup is enclosed with a polyvinyl chloride (PVC) cover to insulate the internal environment from the external surroundings. The enclosure causes a gradual rise in the ambient temperature around the generator during testing. Consequently, a cooling period is required between experiments to allow the test bench to return to and stabilize at the initial ambient temperature.

The prime motor's input speed is set to 5000 r/min, and the stability is monitored via torque sensors. The resistive load is

adjusted to achieve a rectified output power of 3.5 kW from the outer-rotor generator.

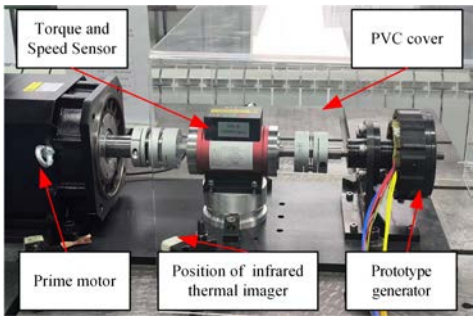

Fig. 13. Experimental platform.

B. Temperature Rise Experiment under Various Conditions

A comparative experiment is conducted to evaluate the cooling performance of the proposed rotor sidewall self-air-cooling structure against the conventional ventilation holes design under load conditions. The test is initiated with both the ambient temperature and the initial generator temperature stabilized at 16 °C.

A temperature rise test is then performed on the generator, with temperature data collected at 2.5-minute intervals. The maximum temperature at the stator outlet end is recorded for each measurement.

Owing to structural constraints, the generator is not rated for prolonged operation at temperatures exceeding 150 °C. Consequently, the experiment is programmed to terminate immediately upon the generator reaching this critical temperature, at which point the generator's operational safety and usability are verified.

The temperature rise test results of the generator under rated operating conditions with different cooling conditions are presented in Fig. 14.

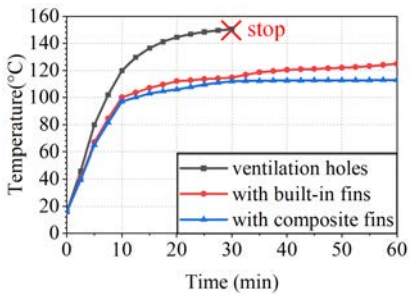

Fig. 14. Experimental results of temperature rise experiment under 5000 r/min.

Under the conventional ventilation hole configuration, the generator rotor temperature rapidly increases to the 150 °C threshold, triggering the protective shutdown mechanism. In contrast, the generator operates stably for 1 h under the two self-air-cooling structures, with temperatures reaching a steady state in both cases. These experimental results clearly validate the superior heat dissipation performance of the proposed self-air-cooling design.

In an external still air environment, both self-cooling structures introduced in this paper demonstrate significantly better cooling performance than the conventional rotor ventilation hole design. Among them, the composite fin structure exhibits the most effective heat dissipation capability.

The cooling performance of the proposed self-cooling structure is highly dependent on the generator's rotational speed. To evaluate this relationship, the generator speed is varied while observing the corresponding cooling effectiveness.

An increase in rotational speed raises the generator voltage, which reduces copper losses in the generator but increases iron losses—an undesirable effect for controlled thermal experiments. To mitigate this, the electrical load is adjusted proportionally with the rotational speed to maintain a constant root mean square (RMS) value of the generator phase current. Under this condition, the temperature of the generator stator remains largely unaffected by variations in experimental parameters.

The prime motor speed is sequentially increased to 5500 and 6000 r/min, while the total operating duration is kept unchanged. The experimental results are presented in Fig. 15.

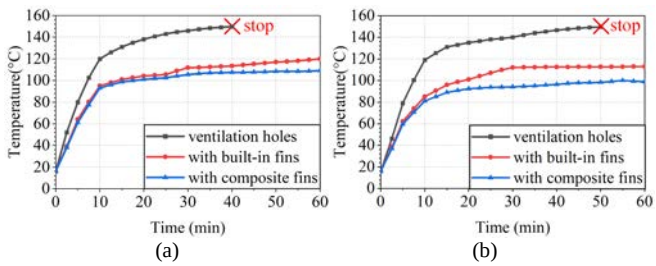

Fig. 15. Experimental results of temperature rise experiment. (a) Under 5500 r/min. (b) Under 6000 r/min

The experimental results indicate that as the rotational speed increases, the cooling advantage of the proposed self-cooling structure becomes more pronounced. Although the stator temperature remains largely constant with the conventional ventilation holes, it exhibits a continuous decrease with the self-cooling structure. This trend confirms that the proposed design achieves significantly enhanced utilization of the rotor's kinetic energy for cooling, thereby demonstrating superior suitability for outer-rotor generator applications.

C. Error Analysis at Rated Speed

To quantify the agreement between experiment and simulation, the error at 5000 r/min is illustrated in Fig. 16.

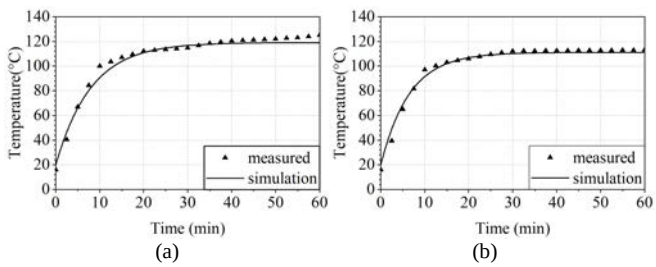

Fig. 16. Discrepancy between experimental and simulation results. (a) With built-in fins. (b) With composite fins.

The comparison shows that the simulated and experimentally measured temperatures at the generator stator

end are in good agreement. Under steady-state conditions, the measured temperature rise exceeds the simulated values by 3 and 1 °C, respectively. The consistent offset between experimental and simulated temperature rise is primarily attributed to the thermal insulation effect of the transparent PVC safety enclosure, which impeded natural convection. Minor contributing factors include slight rotational speed variations due to motor controller tolerance, unmodeled air leakage paths in the assembly, uncertainties in the heater-rotor thermal contact resistance, and the limited accuracy of the infrared thermal camera. However, these external factors cannot be fully considered in the simulation, leading to certain errors in the calculation results.

D. Wind Resistance Loss

Since the designed fins are mounted on the rotor and are easily removable, the additional windage loss introduced by the fins can be quantified using a controlled variable approach. Specifically, the generator stator is removed, and only the rotor is installed on the test bench. The power absorbed is measured sequentially for three configurations: the rotor alone (comprising the disc and shaft system), the rotor with built-in fins, and the rotor with composite fins. The test results are presented in Table IV.

The experimental results indicate that the designed built-in fins and composite fins consume only 20 and 26 W, respectively, at 5000 r/min. This demonstrates that although losses rise with rotational speed, the actual power consumption remains relatively low.

TABLE IV
POWER ABSORBED UNDER DIFFERENT CONDITIONS

Condition	5000 r/min	5500 r/min
Rotor alone/W	136	155
Rotor with built-in fins/W	156	179
Rotor with composite fins/W	162	187

V. CONCLUSION

Two self-air-cooling structures for OR-PMSG are proposed and investigated in this paper. The designs augment the rotating rotor with either built-in fins or composite fins to accelerate airflow within the stator-rotor cavity, thereby enhancing the cooling efficiency of the stator. Theoretical analyses of the two proposed structures are conducted, and their parameters are optimized through fluid-solid-thermal coupling simulations. The main conclusions are as follows:

1) By integrating the self-air-cooling structure directly onto the rotor sidewall, the design effectively addresses spatial constraints. It harnesses rotational energy to generate targeted airflow in the stator-rotor gap, significantly improving stator cooling.

2) The proposed built-in fins substantially increase the circumferential air velocity within the confined generator space, thereby enhancing heat dissipation from the generator stator.

3) By employing an airfoil-shaped design, the composite fins effectively convert rotational energy into axial airflow for internal and external cooling, with verification showing a 9.1% reduction in temperature rise over a conventional flat-plate design.

The experimental results demonstrate the efficacy of the self-cooling structures, showing substantial temperature reductions relative to the conventional design at 5000 r/min: 25.2 °C for the built-in fins and a more pronounced 37.1 °C for the composite fins. This performance improvement is observed to scale with rotational speed.

Therefore, the proposed designs offer a constructive thermal management solution for compact, high-power-density generators operating in external still air environments, such as the ISGs used in small to medium hybrid UAVs, as well as for generators in comparable scenarios with space restrictions. For a geometrically scaled-up system, while the airflow rate may increase, the thermal load and the flow path length also increase, potentially requiring a re-optimization of fin parameters to maintain efficiency. Conversely, for smaller machines, where surface area-to-volume ratio is less favorable and rotational speeds can be very high, the design would focus on minimizing aerodynamic penalty while extracting sufficient cooling flow.

REFERENCES

[1] Y. H. Gai, M. Kimiabeigi, and Y. C. Chong *et al*., "Cooling of Automotive Traction Motors: Schemes, Examples, and Computation Methods," *IEEE Trans. on Ind. Electron.*, vol. 66, no. 3, pp. 1681–1692, Mar. 2019.

[2] C. Liu, Z. Y. Xu, and D. Gerada *et al*., "Experimental Investigation on Oil Spray Cooling with Hairpin Windings," *IEEE Trans. on Ind. Electron.*, vol. 67, no. 9, pp. 7343–7353, Sept. 2020.

[3] P. Shams Ghahfarokhi, A. Podgornovs, and A. Kallaste *et al*., "The Oil Spray Cooling System of Automotive Traction Motors: The State of the Art," *IEEE Trans. on Transport. Electrific.*, vol. 9, no. 1, pp. 428–451, Mar. 2023.

[4] H. M. Wang, X. C. Liu, and M. Kang *et al*., "Oil Injection Cooling Design for the IPMSM Applied in Electric Vehicles," *IEEE Trans. on Transport. Electrific.*, vol. 8, no. 3, pp. 3427–3440, Sept. 2022.

[5] Z. Y. Yu, Y. Li, and Y. T. Jing *et al*., "Cooling System of Outer Rotor SPMSM for a Two-seater All-electric Aircraft based on Heat Pipe Technology," *IEEE Trans. on Transport. Electrific.*, vol. 8, no. 2, pp. 1656–1664, Jun. 2022.

[6] Z. Y. Yu, P. Z. Zhuang, and X. Y. Hu *et al*., "Research on Heat-transfer Characteristics of Cooling System with Heat Pipe Technology for Outer Rotor SPMSM," *IEEE Trans. on Transport. Electrific.*, vol. 11, no. 1, pp. 2866–2876, Feb. 2025.

[7] L. Yan, Z. W. Dong, and S. T. Zhang, "Thermal Analysis of a Novel Linear Oscillating Machine based on Direct Oil-cooling Windings," *IEEE Trans. on Energy Convers.*, vol. 37, no. 2, pp. 1042–1051, Jun. 2022.

[8] A. Acquaviva, S. Skoog, and T. Thiringer, "Design and Verification of In-slot Oil-cooled Tooth Coil Winding PM Machine for Traction Application," *IEEE Trans. on Ind. Electron.*, vol. 68, no. 5, pp. 3719–3727, May 2021.

[9] Y. Liu, Z. Q. Wei, and K. Ma *et al*., "Improved Thermal Management and Analysis for High-power Heat Pipe Cooled FSCW PMSM for HEV Auxiliary Power Unit Application," *IEEE Trans. on Energy Convers.*, vol. 39, no. 2, pp. 1154–1167, Jun. 2024.

[10] B. Y. Bao, B. Xiong, and Z. M. Li *et al*., "Heat Dissipation Characteristics and Experimental Research of Aviation Oil Cooling Motor based on Spiral Insulation Flow Channel Structure in Slot," *IEEE Trans. on Transport. Electrific.*, vol. 11, no. 1, pp. 2322–2331, Feb. 2025.

[11] G. H. Du, H. C. Sun, and Q. Z. Zhang *et al*., "Comparison of

Temperature Characteristics of Outer Rotor LSPMMs Under Different Cooling Structures," *IEEE Trans. on Transport. Electrific.*, vol. 10, no. 4, pp. 9665–9678, Dec. 2024.

[12] K. Rönnberg, Z. Kolondjovski, and C. Duwig, "Analysis of End-winding Heat Transfer in a Low-speed Motor with Forced External Cooling," *IEEE Trans. on Energy Convers.*, vol. 39, no. 1, pp. 160–168, Mar. 2024.

[13] W. Zhang, G. J. Li, and Z. Q. Zhu *et al*., "New Ventilation Cooling for Modular PM Machines Utilizing Flux Gaps and Rotor Ducts," *IEEE Trans. on Energy Convers.*, vol. 39, no. 4, pp. 2718–2727, Dec. 2024.

[14] W. L. Li, Z. B. Cao, and X. C. Zhang, "Thermal Analysis of the Solid Rotor Permanent Magnet Synchronous Motors with Air-cooled Hybrid Ventilation Systems," *IEEE Trans. on Ind. Electron.*, vol. 69, no. 2, pp. 1146–1156, Feb. 2022.

[15] Y. L. Bi, F. Chai, and L. Chen, "The Study of Cooling Enhancement in Axial Flux Permanent Magnet Motors for Electric Vehicles," *IEEE Trans. on Ind. Appl.*, vol. 57, no. 5, pp. 4831–4839, Sept.-Oct. 2021.

[16] H. Vansompel, and P. Sergeant, "Extended End-winding Cooling Insert for High Power Density Electric Machines with Concentrated Windings," *IEEE Trans. on Energy Convers.*, vol. 35, no. 2, pp. 948–955, Jun. 2020.

[17] F. Y. Zhang, D. Gerada, and Z. Y. Xu *et al*., "Back-iron Extension Thermal Benefits for Electrical Machines with Concentrated Windings," *IEEE Trans. on Ind. Electron.*, vol. 67, no. 3, pp. 1728–1738, Mar. 2020.

[18] J. Q. Xiao, K. Uvodich, and C. Z. Fu *et al*., "Modeling and Optimization of Self-pumping Air-cooled Thermal Management System for a High Specific Power Outer Runner Electric Motor," in *Proc. of 2025 IEEE International Electric Machines & Drives Conference*, Houston, TX, USA, May 2025, pp. 164–169.

[19] A. Bejan, S. Lorente, and J. Lee *et al*., "Constructal Design of Gas-cooled Electric Power Generators, Self-pumping and Atmospheric Circulation," *International Journal of Heat and Mass Transfer*, vol. 9, pp. 647–655, Dec. 2015.

[20] W. Le, M. Y. Lin, and K. M. Lin *et al*., "Design and Analysis of a Rotor Air-cooling Enhanced Method for Axial Flux Permanent Magnet Machine with Housing-cooling," *IEEE Trans. on Energy Convers.*, vol. 38, no. 3, pp. 2136–2145, Sept. 2023.

[21] M. Liben, and D. C. Ludois, "Analytical Design and Experimental Testing of a Self-cooled, Toroidally Wound Ring Motor with Integrated Propeller for Electric Rotorcraft," *IEEE Trans. on Ind. Appl.*, vol. 57, no. 3, pp. 2342–2353, May-Jun. 2021.

[22] Y. Kai, and F. Yaojing, "Design of Novel Spiral Magnetic Poles and Axial-cooling Structure of Outer-rotor PM Torque Motor," *IEEE Trans. on Appl. Supercond.*, vol. 20, no. 3, pp. 838–841, Jun. 2010.

[23] H. Shi, Q. Chen, and J. H. Liao *et al*., "Design and Optimization of Dual-air Duct Cooling System for Rotor Permanent Magnet Flux-switching Motor," *IEEE Trans. on Transport. Electrific.*, vol. 11, no. 2, pp. 7029–7039, Apr. 2025.

[24] T. H. Blair, "FANS," in *Energy Production Systems Engineering*, U.S.: Wiley-IEEE Press, 2017, pp. 175–187.

Sirui Wang received the B.E. degree in 2021 from the Harbin Institute of Technology, Harbin, China, where he is currently working toward the Ph.D. degree in electrical engineering. His current research interests include the design and thermal model calculation of permanent magnet Integrated Starter-Generator Motors.

Fangrui Wei (1993.12–) received the B.Eng. and M.Sc. degrees in electrical engineering from Harbin Institute of Technology, Harbin, China, in 2016 and 2018, respectively, and Ph.D. degree from the University of Sheffield, Sheffield, UK. He is currently working as a lecture at Harbin Institute of Technology, Harbin, China. His current research interests include the design and analysis of permanent magnet machines and thermal management in electric machines.

Yong Li was born in Heilongjiang, China, in 1964. He received the Ph.D. degree in electrical engineering from Harbin Institute of Technology, Harbin, China, in 1988. He is currently a Professor in the Department of Electrical Engineering in Harbin Institute of Technology, Harbin, China.

His research interests include PMSMs, special motors, and their applications.

JianHui Hu was born in 1975, Associate Professor, Department of Electrical Engineering, Harbin Institute of Technology, Harbin, China. He received the Ph.D. degree in electrical engineering from Harbin Institute of Technology, Harbin, China, in 2005.

His research interests include special electrical machines and electrical drives.

Qian Wang was born in 1982 in Henan, China. He received his Ph.D. degree in electrical engineering from the Harbin Institute of Technology in 2010. He is now an associate professor in the Department of Electrical Engineering, Harbin Institute of Technology, Harbin, China.

Pengcheng Ma was born in 1994 in Shandong, China. He received his Ph.D. degree in electrical engineering from the Harbin Institute of Technology, Harbin, China, in 2022. He is now a research assistant in the Chinese Academy of Sciences Aerospace Information Research Institute, Beijing, China.